LOW-TEMPERATURE PLASMA

High-Frequency Discharge with a Jet Electrolytic Electrode

Al. F. Gaisin[a, *], **F. M. Gaisin**[a], **V. S. Zheltukhin**[a], and **E. E. Son**[b]

[a] *Tupolev Kazan National Research Technical University−KAI, Kazan, 420111, Russia*
[b] *Joint Institute for High Temperatures, Russian Academy of Sciences, Moscow, 125412 Russia*
*e-mail: almaz87@mail.ru

Abstract—A high-frequency discharge (f = 13.56 MHz) generated between jet electrolytic (3% solution of ammonium sulfate in purified water) and metal (copper plates of the M1 grade) electrodes in the pressure range of $p = 10^5-3 \times 10^4$ Pa is studied. The ignition of the high-frequency (HF) discharge was carried out by applying an electrolyte jet to the surface of a copper plate in the discharge chamber. The types and shapes of plasma structures generated in the interelectrode gap and their mutual transformations at the change in the voltage are considered. Hydrogasdynamic processes in the combustion zone of the HF discharge are described, including optically inhomogeneous gas flows, disturbances of the jet electrode, and the formation of droplets. The thermograms of the surface of the jet and metal electrodes under the conditions of the HF discharge combustion are considered. The composition of the plasma, the electron density, and the temperature of the heavy component are studied using emission spectroscopy.

1. INTRODUCTION

Gas discharge plasma with liquid (non-metallic) electrodes is a rapidly developing interdisciplinary field of research, including the science of plasma, fluid dynamics, heat and mass transfer, multiphase chemistry, and photolysis [1]. Unlike discharges between solid electrodes (glow, arc, spark, corona discharges, etc.) [2], discharges in plasma-liquid systems are generated by direct or alternating current in the interelectrode gap, where one or both electrodes are a flowing or non-flowing liquid [3]. As a rule, solutions of salts of various concentrations in industrial, distilled or tap water are used as a liquid electrode. Tap water is subjected to preliminary purification in order to eliminate fluctuations during the experiment due to the composition tap water. The discharge is ignited in plasma-liquid systems at various types and configurations of electrodes in the gas-discharge chamber. The discharge with jet electrodes is studied in the jet, jet-droplet and droplet modes of the electrolyte flow.

A great deal of interest in the low-temperature plasma of discharges of plasma-liquid systems is associated with their successful application for the surface treatment of products [4−7], preparation of nanoparticles [8−10], application of functional coatings [11, 12], estimate of the content of particles in a liquid [13, 14], plasma reactors [15, 16], production of fine powders used in additive technologies [17], water and air purification [18]. A wide variety of applications of such discharges is associated with a large number of possible configurations of discharge chambers, modes and parameters of discharge ignition and combustion, as well as common plasma-chemical processes associated with the transfer of matter and charge at the phase interface [19, 20].

Sakiyama et al. [21] found that in physicochemical processes occurring in plasma-liquid systems, there are more than 50 charged and neutral atomic and molecular particles that react with each other and affect the energy balance in the discharge.

Direct current electric discharges with liquid electrodes at atmospheric pressure were studied in [22−24]. It was found that the discharge stably burns in air at atmospheric pressure in a diffuse (volumetric) form in an interelectrode gap of 4−10 mm when powered with a constant current of 40−100 mA and at a current density of $\sim 10^4$ A/m². It was revealed that the discharge is divided into two near-electrode regions and an almost uniform column. It was found that the discharge generates a substantially nonequilibrium plasma: the gas temperature ≈2000 K in the discharge column, the electron temperature (average energy) of ≈4500 K, and electron density of ≈10^{18} m^{-3}.

Optical emission spectroscopy methods were used to diagnose the plasma parameters with liquid electrodes [25]. Strong emission of OH (A−X) and hydrogen lines at the contact of plasma with liquid was
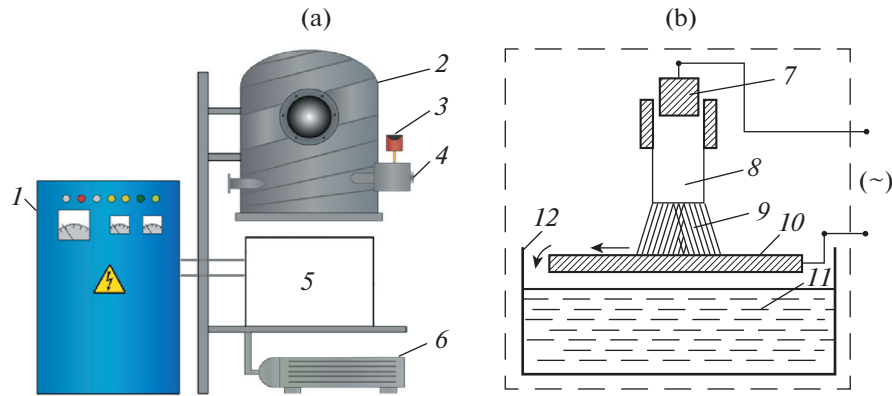
Fig. 1. Schemes of (a)—experimental setup and (b)—gas discharge chamber: *1*—HF generator; *2*—vacuum chamber; *3*—vacuum gauge; *4*—valve for supplying air to the chamber; *5*—working region with a gas-discharge chamber; *6*—vacuum pump; where: *7*—metal electrode for applying the potential into the electrolyte jet; *8*—dielectric tube for applying the electrolyte jet; *9*—electrolyte jet; *10*—copper electrode; *11*—electrolyte; and *12*—electrolytic bath.

revealed. The electron density was determined in the range of 10^{21}–10^{23} m^{-3} from two hydrogen H_α and H_β lines.

Electrical destruction and deformation of the water surface between the metal and liquid electrodes were studied for small interelectrode distances (2–12 mm) [26]. The calculations of the deformation of the water surface depending on the applied voltage and the initial interelectrode spacing were presented. The calculation results are compared with measurements of the water height. The calculated stability limit of the water surface corresponds to the experimental breakdown voltage for distances less than 7 mm. The water surface has a Taylor cone shape at the destruction. The breakdown voltage at the interelectrode distance of 7 mm and higher is significantly lower than the water stability limit, and the conducting channel during the breakdown is formed between the electrode pin and the static surface of water.

The effect of the conductivity of water on the electrospraying of water in combination with a corona discharge generated in air was studied in [27]. The authors used a point-to-plane electrode geometry with an anode in the form of a hollow syringe needle opposite to the cathode of the metal grid. Different jets were observed depending on the conductivity: pointed, elongated and rapidly expanding water filaments for lower conductivity unlike the round, wider, and shorter rapidly decaying filaments for higher conductivity.

The analysis of publications shows that plasma-liquid systems have been studied for a long time, however, the number of "white spots" in this field of science is still large. For example, HF current discharges with liquid electrodes are still studied poorly [29], while the scientific foundations of HF discharges with solid electrodes are described in detail in the well-known works of Yu.P. Raizer et al. [2, 28].

The purpose of this work is to study the properties of an HF discharge ignited between jet electrolytic and metal electrodes. The results of this work can be used for the development of mathematical models of HF discharges with liquid electrodes and for engineering methods of calculation of plasma facilities.

2. EXPERIMENTAL SETUP AND RESEARCH METHODS

Figure 1 shows a functional diagram of the experimental setup with a gas-discharge chamber for ignition and maintenance of an HF discharge in the considered configuration of electrodes. The HF discharge was studied at the following set parameters: voltage $U = 0.1$–5 kV, pressure $p = 10^5$–10^4 Pa, jet flow velocity $v_j = 0.05$–0.6 m/s, jet length $l_j = 7$–30 mm, jet diameter $d_j = 7$–30 mm, a copper plate of the M1 grade with a diameter $d_s = 3$–10 mm was used as a metal electrode, and a 3% solution of ammonium sulfate in purified tap water was used as an electrolyte.

The process of ignition of an HF discharge in a gas-discharge chamber (Fig. 1b) is as follows: an electrolyte jet *9* is applied to the surface of the copper electrode *10* from a dielectric tube *8*. Preliminarily, a metal electrode *7* is placed in the dielectric tube *8* to apply a potential to the electrolyte jet *9*. After the potential is applied on the electrodes, the discharge is formed along the electrolyte jet *9* and at the interface between the copper plate *10* and the electrolyte jet *9*, then the liquid flows into the electrolytic cell *12* with electrolyte *11*. A thermostat is provided to control the temperature of the electrolyte solution in the bath. The electrolyte is thermostated using a refrigerator-type circulation cooler. The electrolyte in the bath is renewed using an electrolyte supply and pumping system. A coarse filter is provided in the system in order to clean the solution from impurities. Electrolyte

vapors are removed from the region, where the discharge is studied, using a stationary hood and a fan.

The electrolyte jet was applied from an electrolytic cell with a free surface; the flow is pressureless. The jet velocity v_j was changed using a control valve and was calculated according to the formula $v_j = G/\rho S = G/\rho\pi(d/2)^2$, where G is the electrolyte consumption, S is the cross section area and ρ is the density of liquid. Dielectric tubes of different diameters were used to change the jet diameter v_j.

The vacuum system of the experimental setup consists of a vacuum chamber, a 2NVR-5DM brand vacuum pump and a VTI 1218 vacuum gauge of 0.6 accuracy class. A cylindrical vacuum chamber with a volume of 0.12 m^3 is made of steel, and the dimensions of the working zone are 500 × 640 mm. The vacuum chamber has two optical glass windows. The vacuum chamber is connected to the pumping, pressure measuring and regulating system via vacuum flanges. Electrical connectors for connecting electrodes to the HF generator are located on the plate of the vacuum chamber.

A VChG8-60/13 HF generator with an operating frequency of 13.56 MHz is used as a power source. Additional connectors for connecting the diagnostic equipment are also located on the plate. The working pressure in the vacuum chamber is controlled by changing the pumping rate and by the leak valve for air injection. The vacuum chamber is elevated and lowered using a hydraulic drive.

The tasks indicated in the work are solved by using modern diagnostic equipment, research methods and approaches:

1. Video recording of the dynamics of the processes occurring in the zone of the high-frequency discharge combustion, as well as the plasma structures formed in this case, was carried out using a Casio EX-F1 high-speed video camera. In view of the high dynamics of the processes occurring in the zone of the discharge combustion, the shooting rate was chosen at 1200 and 600 frames per second. The camera was mounted on a tripod at a distance of 300 mm from the zone of the discharge combustion and transmitted the obtained information to a computer with an operator. The data were processed on a personal computer using the HX Link and Movavi Video Editor 14 Plus software [30]. An additional detailed study of the plasma structures on the surface of the liquid and metal electrodes was carried out simultaneously on an SP-52 microscope.

2. Spatial visualization of gas-hydrodynamic processes in the zone of the high-frequency discharge combustion was carried out on a facility that implements the Schlieren method (Toepler method). The advantage of this method is the ability to visualize the weakest optical inhomogeneities.

3. The emission spectrum of the high-frequency discharge plasma was analyzed by emission spectroscopy on a PLASUS EC 150201 MC fiber-optic spectrometer. The discharge emission was recorded using a collimator for fixing light beams in the wavelength range of 195−1105 nm. The collimator was brought to the zone of the discharge combustion at a distance of 100−200 mm. The system apparatus function was calibrated by recording light emission from a SIRSH 6-100 lamp. The width of the minimum, single and narrowest spectral lines, which was $\Delta\lambda g = 1$ nm, was taken as the apparatus width. The studied emission was collected from the total volume of the discharge, therefore, the composition and components of the plasma were estimated without reference to a specific point in the discharge. The obtained data were analyzed by comparing the studied spectrum with the National Institute of Standards and Technology database (NIST, the United States). The vibrational and rotational temperatures of the heavy plasma component were determined by comparing the experimental molecular spectrum with the model calculated in the LIFBASE [31] and Specair 2.2.0.0 [32] packages.

4. A FLIRA6500SC thermal imaging camera with a detector spatial resolution of 640 × 512 pixels with a working spectral range of 3.6−4.9 μm was used to analyze the temperature distribution of the studied surface of the metal and electrolytic electrodes during the combustion of the HF discharge. The thermal imager provided recording of the electrode surface temperature in the calibrated range of 4−2400°C. A multiwave pyrometer was used to calibrate the thermal imaging camera. The use of the pyrometer was due to the fact that an oxide film and scale can be formed during the discharge combustion, which can lead to errors in the measured temperature. The obtained data were processed on a computer with the ALTAIR v5.91.010 software.

5. The current and voltage fluctuations of the HF current discharge were studied on an AKTAKOM ASK-2067 digital oscilloscope with a high-frequency "Elektronika R6015A" voltage divider.

3. DISCUSSION OF RESULTS

A study of the initiation of an HF discharge at atmospheric pressure by the contact method of an electrolytic jet electrode with the surface of the copper plate showed that when a voltage is applied in the range from 100 to 1000 V, electrolyte evaporation occurs at the boundary with the formation of vapor-air bubbles of various diameters. The current, which passes in the circuit, triggers the Joule heat release from the surface of the copper plate and the physico-chemical release of solutes from the electrolyte that is characteristic of electrolysis. The course of electrolysis is determined by the transport of the electric current in the liquid and the conditions of recombination of the electrolyte ions present in the solution. By changing the composition, concentration and temperature of the electrolyte, it is possible to change the course of
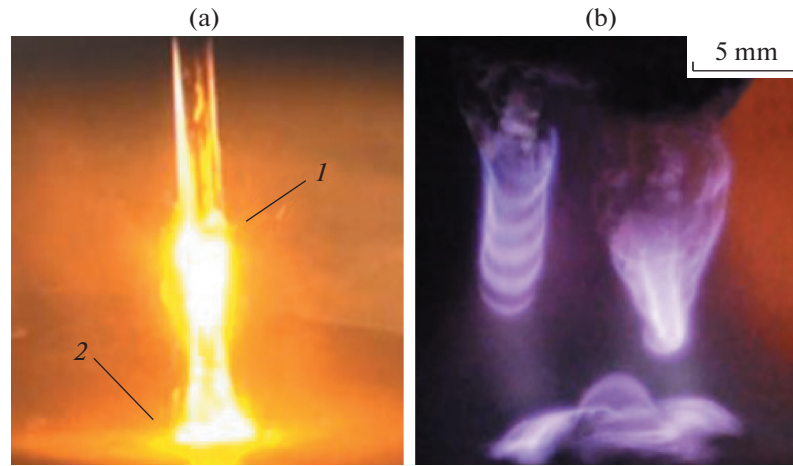
Fig. 2. Photographs of the HF discharge combustion between the jet electrolytic and metal electrodes at (a) atmospheric and (b) reduced pressures, where *1*—jet decay zone; *2*—contact region of the jet with the surface of the metal electrode.
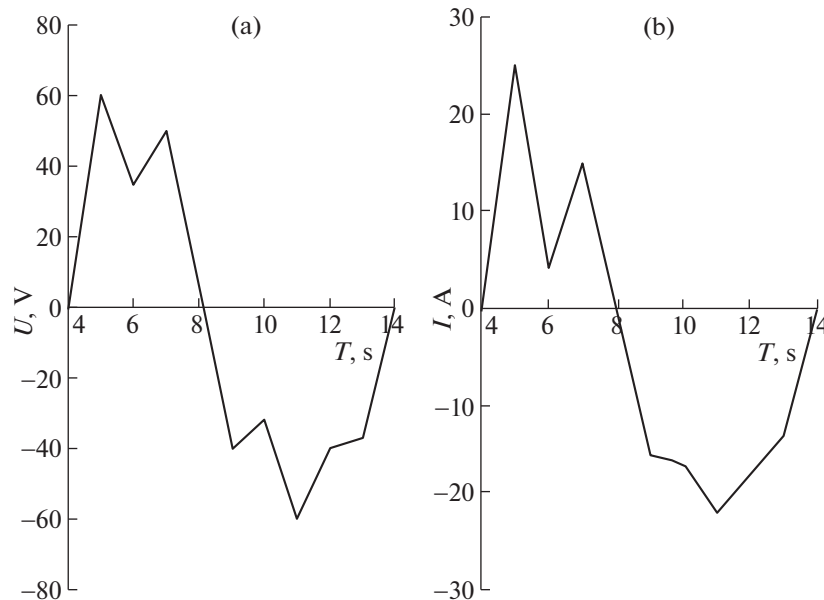

Fig. 3. Oscillogram of a (a) voltage and (b) current oscillation of the electric discharge of the HF current between liquid and copper electrodes.

the electrode processes in the desired direction. At the same time, no breakdown is observed, since the power applied to the discharge remains insufficient to ionize the vapor-air medium and initiate an electron avalanche. It follows from the analysis of the oscillograms that at no-load, the current value is of 12–14 A.

When the voltage increases from 1000 to 2500 V, the intensity of the processes occurring in the interelectrode gap increases, and the solution on the surface of the metal electrode begins to boil. A phase interphase appears in the volume of the electrolyte with the formation of a vapor-air shell on the surface

of the copper plate. At some time, the electric field strength reaches values sufficient for the breakdown of the gas gap between the electrodes. As a result of the breakdown at the interface between the media, microdischarges appear in the form of current pulses with the amplitude of 12 to 16 A.

When the voltage increases from 2.5 to 4 kV, the discharge turns into a stable combustion mode, while the current increases to 18–25 A. Microdischarges are formed as truncated yellow cones, the tops of which rest on the surface of the falling droplet, and the bases rest on the surface of the copper electrode (Fig. 2a).
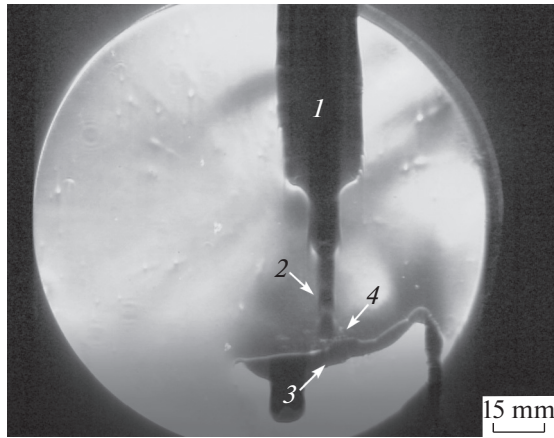
Fig. 4. Schlieren image of hydrogasdynamic processes in the zone of the HF discharge combustion between the jet electrolytic and copper electrodes: *1*—dielectric tube for applying the electrolyte jet; *2*—electrolyte jet; *3*—copper electrode; and *4*—zone of the electric discharge combustion.

It was established that the discharge is mainly formed in two zones of the jet: *1*—in the zone of the jet decay and *2*—in the contact region of the jet with the surface of the metal electrode. A further increase in the applied voltage to 5 kV and higher leads to the breakdown between the conductive plate in the electrolytic bath *7* and the copper plate *10* with the formation of the arc and excessive load on the HF generator lamp.

When the pressure in the vacuum chamber decreases to 10^4 Pa, the HF discharge combustion is characterized by the higher intensity, lower breakdown voltage and the formation of the ring and semi-ring plasma structures along the jet electrode (Fig. 2b).

The analysis of the voltage and current oscillations of the HF discharge showed that the oscillations on the grounded electrode occur with two current and voltage pulsations, while the oscillations on the loaded electrode occur with three current and voltage pulsations (Fig. 3).

Spatial visualization of hydrogasdynamic processes in the zone of the high-frequency discharge combustion between the electrolytic and copper jet electrodes at atmospheric pressure was carried out on the facility that implements the schlieren method (Fig. 4). It was established that when a jet is applied to a copper electrode, a breakdown occurs with the HF discharge combustion. A region of intense mixing of liquid, gas and plasma is observed in the zone of the HF discharge combustion. This process is accompanied by intense evaporation of the electrolyte, the formation of droplets and the release of convective vapor-gas flows, where dark regions correspond to a shock wave, and light regions to rarefaction.

The zone of the HF discharge combustion between the jet electrolytic and copper electrodes at atmospheric pressure was studied using a thermal imager (Fig. 5). It follows from the analysis of the thermograms that the temperature of the electrolyte on the
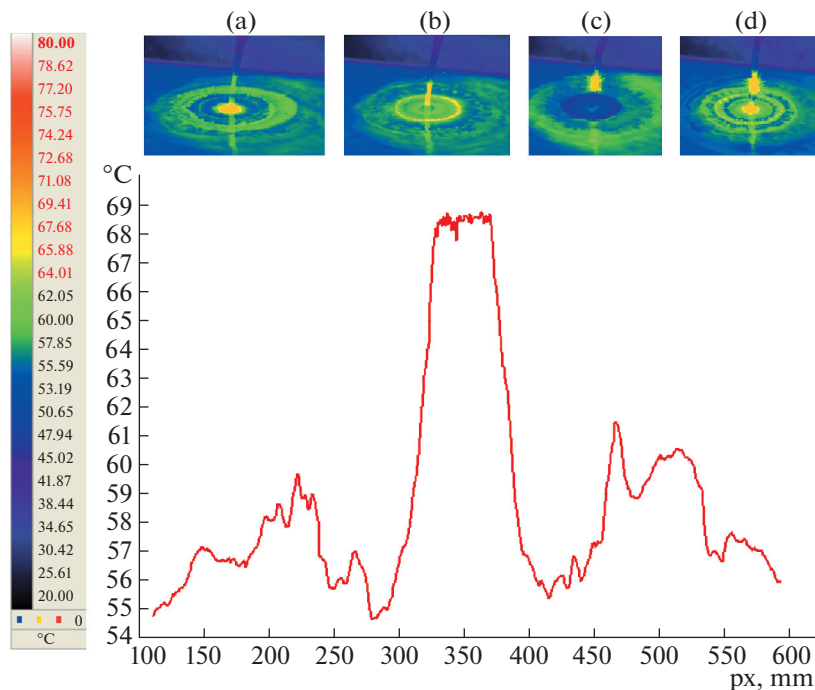

Fig. 5. Thermogram of the surface of a copper plate in the zone of the HF discharge combustion with a jet electrolytic electrode, where (a) before the breakdown; (b) jet narrowing; and (c, d) discharge breakdown and combustion.
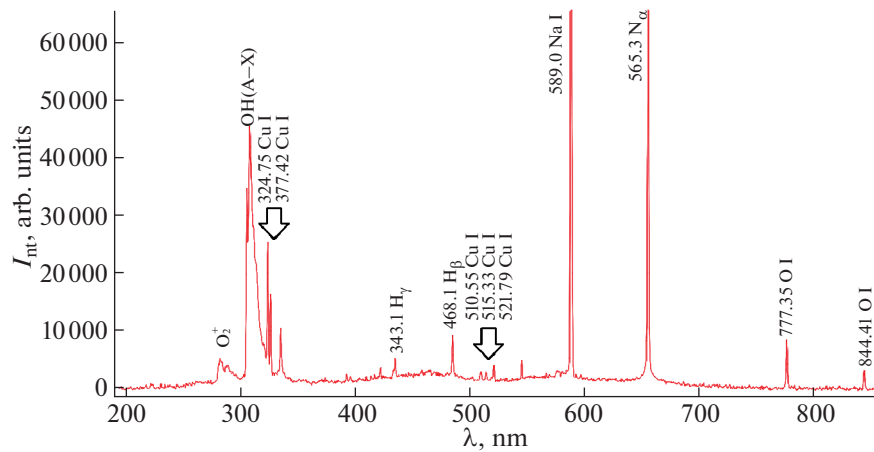
Fig. 6. Spectrum under study with identified spectral lines.

surface of the copper electrode in the zone of the discharge combustion reaches ~69°C, then the temperature of the electrolyte changes cyclically, which is associated with the periodic passage of volumes of hot and cold liquid.

The analysis of the spectra of the HF discharge plasma showed that the observed region contains various elements: hydrogen H I, sodium Na I, copper Cu I, oxygen O I atoms, molecular oxygen O_2^+ ions and hydroxyl OH (A−X) (Fig. 6). The electron density in the plasma of the HF current discharge was estimated by analyzing the contours of the hydrogen H_β lines. The width of the Voigt contour of the hydrogen H_β line is determined. It corresponds to $\Delta\lambda_f = 1.25$ nm at its half-height. The Lorentzian component of the recorded line taking into account the apparatus broadening under the assumption of the Voigt contour is $\Delta\lambda_L = 0.43$ nm. The quantity $\Delta\lambda_L$, which is due to the linear Stark effect, corresponds to the electron density of $n_e = 3.06 \times 10^{15}$ cm^{-3}.

The methods for determining the electron temperature used for the estimates assume the presence of the local thermodynamic equilibrium state in the plasma. It is difficult to determine the electron temperature from the above spectra, since the data on atomic (and) or ionic lines do not suffice. The vibrational T_v and rotational T_r temperatures were determined for the OH (A−X) molecular band. The best match for the OH (A−X) molecular band was obtained at temperatures in the ranges of $T_v = 3450$–3570 K and $T_r = 4680$–4870 K.

4. CONCLUSIONS

As a result of experimental and theoretical studies of the electric HF current discharge ($f = 1356$ MHz) between jet electrolytic and metal electrodes in a wide pressure range, it was established that different ele-

ments: hydrogen H I, sodium Na I, copper Cu I, oxygen O I atoms, molecular oxygen O_2^+ ions and hydroxyl OH (A−X) are present in the observed plasma region. The electron density obtained from the analysis of hydrogen lines of the Balmer series is $n_e = 3.06 \times 10^{15}$ cm^{-3}. The rotational temperature $T_v = 3450$–3570 K and vibrational temperature $T_r = 4680$–4870 K were obtained by comparing the molecular spectrum with the model spectrum for the OH (A−X) band.

CONFLICT OF INTEREST

The authors declare that they have no conflicts of interest.

REFERENCES

1. P. J. Bruggeman, M. J. Kushner, B. R. Locke, J. G. E. Gardeniers, W. G. Graham, D. B. Graves, R. C. H. M. Hofman-Caris, D. Maric, J. P. Reid, E. Ceriani, D. Fernandez Rivas, J. E. Foster, S. C. Garrick, Y. Gorbanev, S. Hamaguchi, et al., Plasma Sources Sci. Technol. **25**, 053002 (2016). https://doi.org/10.1088/0963-0252/25/5/053002

2. Yu. P. Raizer, *Gas Discharge Physics,* Ed. by J. E. Allen (Springer-Verlag, Berlin, 1991), Vol. 1, p. 449.

3. N. Kashapov, R. Kashapov, and L. Kashapov, J. Phys. D: Appl. Phys. **51**, 494003 (2018). https://doi.org/10.1088/1361-6463/aae334

4. E. I. Meletis, X. Nie, F. L. Wang, and J. C. Jiang, Surf. Coat. Technol. **150**, 246 (2002). https://doi.org/10.1016/S0257-8972(01)01521-3

5. T. Ishijima, K. Nosaka, Y. Tanaka, Y. Uesugi, Y. Goto, and H. Horibe, Appl. Phys. Lett. **103**, 142101 (2013). https://doi.org/10.1063/1.4823530

6. Al. F. Gaysin, Inorg. Mater.: Appl. Res. **8**, 392 (2017).
https://doi.org/10.1134/S207511331703008X

7. A. F. Gaysin, A. K. Gil'mutdinov, and D. N. Mirkhanov, Met. Sci. Heat Treat. **60**, 128 (2018).
https://doi.org/10.1007/s11041-018-0250-1

8. R. Wüthrich and A. Allagui, Electrochim. Acta **55**, 8189 (2010).
https://doi.org/10.1016/j.electacta.2010.01.096

9. T. A. Kareem and A. A. Kaliani, Ionics **18**, 315 (2012).
https://doi.org/10.1007/s11581-011-0639-y

10. G. Saito, S. Hosokai, M. Tsubota, and T. Akiyama, J. Appl. Phys. **110**, 023302 (2011).
https://doi.org/10.1007/s11090-011-9313-4

11. T. Paulmier, J. M. Bell, and P. M. Fredericks, Thin Solid Films **515**, 2926 (2007).
https://doi.org/10.1016/j.tsf.2006.08.027

12. C. Quan and Y. He, Surf. Coat. Technol. **269**, 319 (2015).

13. P. Mezei, T. Czerfalvi, and M. Jánossy, J. Phys. D: Appl. Phys. **31**, L41 (1998).
https://doi.org/10.1088/0022-3727/31/11/001

14. M. Smoluch, P. Mielczarek, and J. Silberring, Mass Spectrom. Rev. **35**, 22 (2016).
https://doi.org/10.1002/mas.21460

15. K. H. Becker, K. H. Schoenbach, and J. G. Eden, J. Phys. D: Appl. Phys. **39**, R55 (2006).
https://doi.org/10.1088/0022-3727/39/3/R01

16. J. Gao, D. Ma, Q. Lu, Y. Li, X. Li, and W. Yang, Plasma Chem. Plasma Process. **30**, 873 (2010).
https://doi.org/10.1007/s11090-010-9251-6

17. R. Kashapov, L. Kashapov, and N. Kashapov, J. Phys.: Conf. Ser. **927**, 012086 (2017).
https://doi.org/10.1088/1742-6596/927/1/012086

18. E. E. Son, R. Sh. Sadriev, Al. F. Gaisin, L. N. Bagautdinova, F. M. Gaisin, E. F. Shakirova, M. F. Akhatov, Az. F. Gaisin, and R. R. Kayumov, High Temp. **52**, 939 (2014).
https://doi.org/10.1134/S0018151X14060169

19. P. Bruggerman and C. Leys, J. Phys. D: Appl. Phys. **42**, 053001 (2009).
https://doi.org/10.1088/0022-3727/42/5/053001

20. S. Samukawa, M. Hori, S. Rauf, K. Tachibana, P. Bruggeman, G. Kroesen, J. C. Whitehead, A. B. Murphy, A. F. Gutsol, and S. Starikovskaia, J. Phys. D: Appl. Phys. **45**, 253001 (2012).
https://doi.org/10.1088/0022-3727/45/25/253001

21. Y. Sakiyama, D. B. Graves, H.-W. Chang, T. Shimizu, and G. E. Morfill, J. Phys. D: Appl. Phys. **45**, 425201 (2012).
https://doi.org/10.1088/0022-3727/45/42/425201

22. P. André, Y. Barinov, G. Faure, and S. M. Shkol'nik, J. Phys. D: Appl. Phys. **44**, 375203 (2011).
https://doi.org/10.1088/0022-3727/44/37/375203

23. P. André, Y. Barinov, G. Faure, and S. M. Shkol'nik, J. Phys. D: Appl. Phys. **44**, 375202 (2011).
https://doi.org/10.1088/0022-3727/44/37/375202

24. Al. F. Gaisin, N. F. Kashapov, A. I. Kuputdinova, and R. A. Mukhametov, Tech. Phys. **63**, 695 (2018).

25. P. Bruggeman, T. Verreycken, M. Á. González, J. L. Walsh, M. G. Kong, C. Leys, and D. C. Schram, J. Phys. D: Appl. Phys. **43**, 124005 (2010).
https://doi.org/10.1088/0022-3727/43/12/124005

26. P. Bruggeman, L. Graham, J. Degroote, J. Vierendeels, and C. Leys, J. Phys. D: Appl. Phys. **40**, 4779 (2007).
https://doi.org/10.1088/0022-3727/40/16/007

27. B. Pongrác, H.-H. Kim, N. Negishi, and Z. Machala, Eur. Phys. J. D **68**, 224 (2014).
https://doi.org/10.1140/epjd/e2014-50052-4

28. Yu. P. Raizer, M. N. Shneider, and N. A. Yatsenko, *Radio-Frequency Capacitive Discharge* (Moscow, Nauka, 1995; CRC, London, 1995).

29. Al. F. Gaisin, E. E. Son, and S. Yu. Petryakov, Plasma Phys. Rep. **43**, 741 (2017).
https://doi.org/10.1134/S1063780X17070054

30. Movavi software packages. https://www.movavi.ru/. Cited May 20, 2021.

31. LIFBASE 2.0: Database and Spectrum Simulation. https://lifbase.software.informer.com/2.0/. Cited May 20, 2021.

32. Specair: Spectral Fitting Made Easy. http://spectral-fit.com/. Cited May 20, 2021.

Translated by L. Mosina